Electronic Supplementary Material (ESI) for Physical Chemistry Chemical Physics.

Supplementary Information

The Role of Copper in The Thermal Conductivity of Thermoelectric Oxychalcogenides: Do Lone Pairs Matter?

P. Vaqueiro,[a*] R. A. R. Al Orabi,[b] S. D. N. Luu,[a,c] G. Guélou,[a] A. V. Powell,[a] R. I. Smith,[d] J.-P. Song,[b] D. Wee[b] and M. Fornari[e*]

[a.] *Department of Chemistry, University of Reading, Whiteknights, Reading, RG6 6AD, UK. E-mail: p.vaqueiro@reading.ac.uk*

[b.] *Department of Environmental Science and Engineering, Ewha Womans University, Seoul, South Korea.*

[c.] *Institute of Chemical Sciences, Heriot-Watt University, Edinburgh, EH14 4AS, UK*

[d.] *ISIS Facility, Rutherford Appleton Laboratory, Harwell, Oxford, Didcot, OX11 0OX, UK*

[e.] *Department of Physics, Central Michigan University, Mt. Pleasant, MI 48859, USA. E-mail: marco.fornari@cmich.edu*

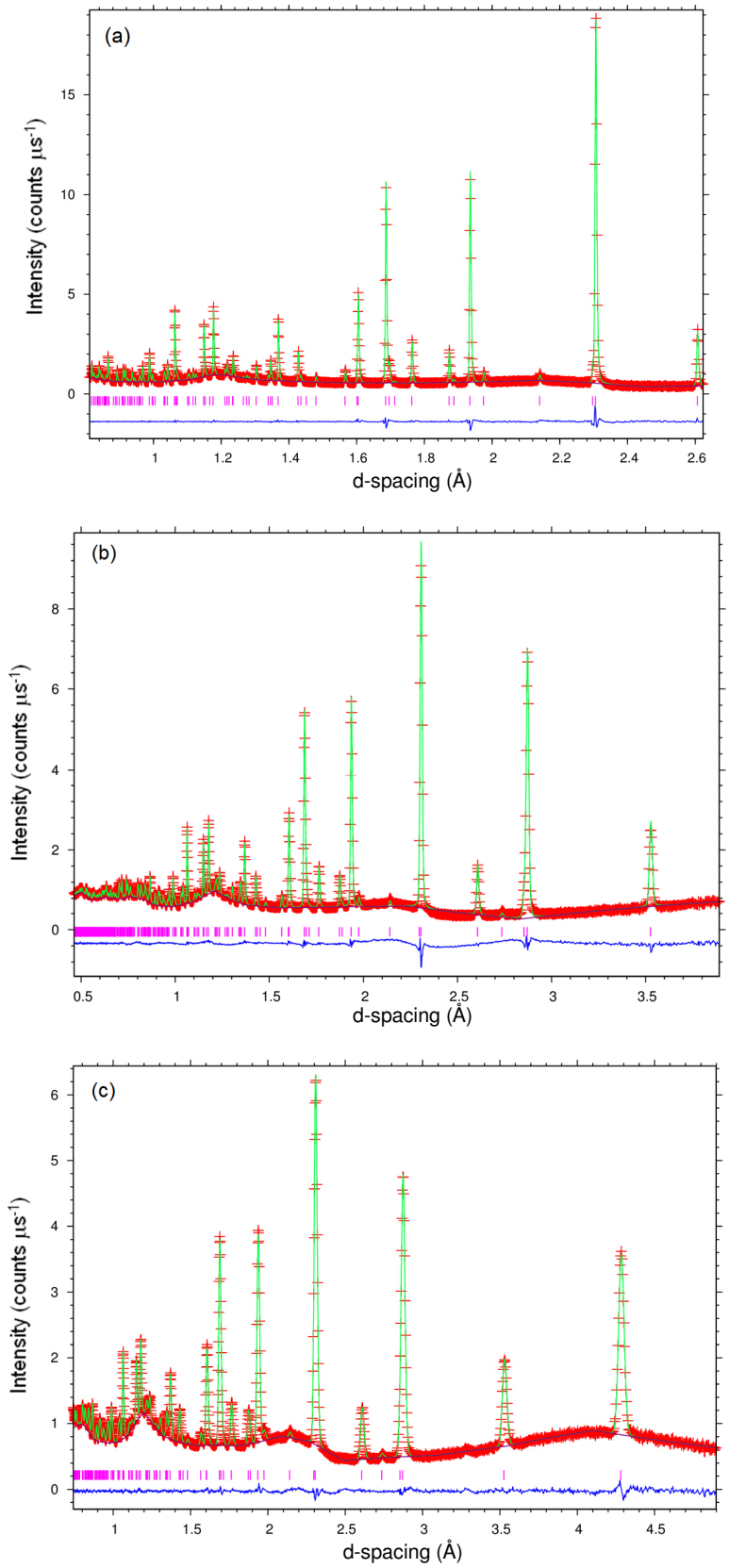

Figure S1. Rietveld refinement using powder neutron diffraction data collected on POLARIS for BiOCuS at room temperature from (a) backscattering bank (b) 90° bank and (c) low angle bank (average 2θ = 146.7°, 92.6 ° and 52.21° respectively). Key: observed data (red cross); difference curve (blue line); calculated pattern (green line); background (black line) and reflection positions (pink markers).

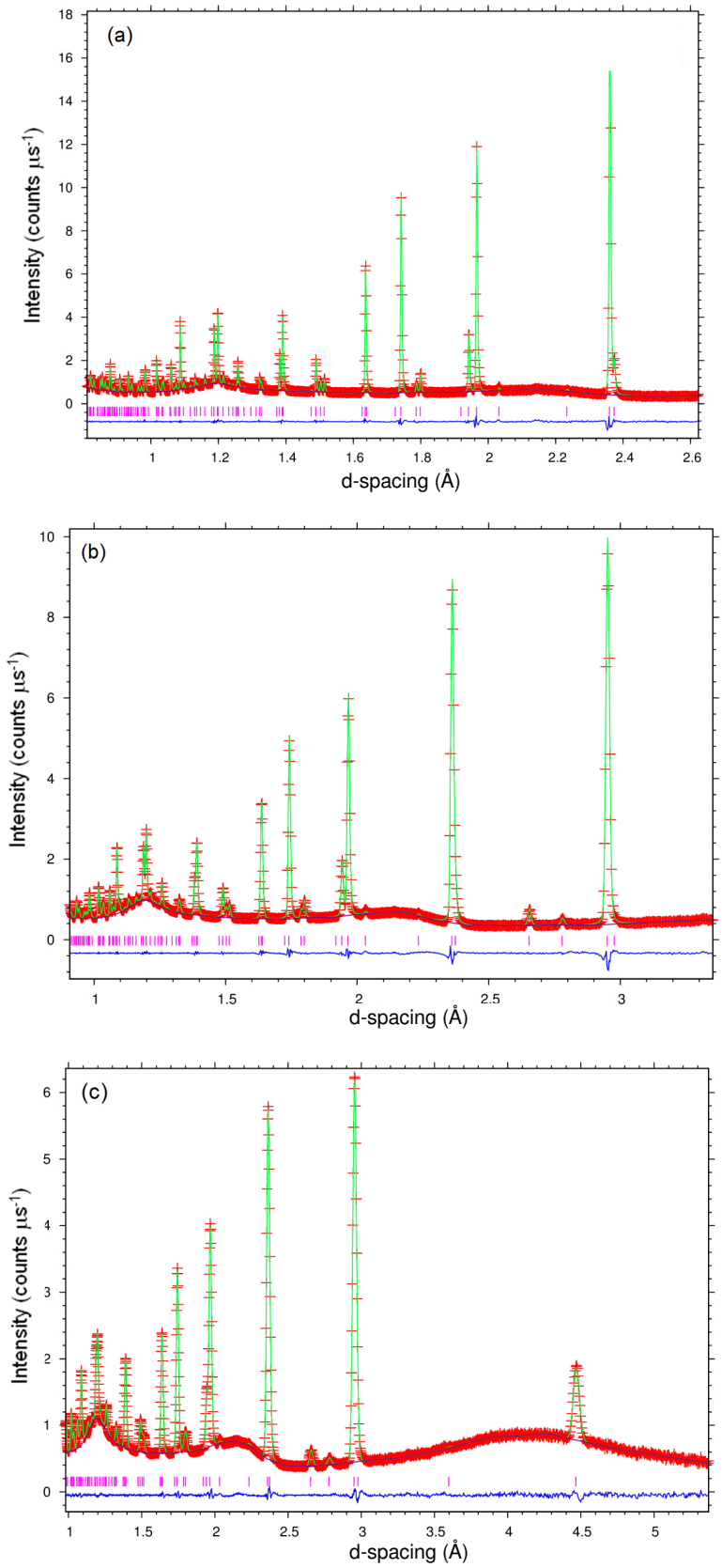

Figure S2. Rietveld refinement using powder neutron diffraction data collected on POLARIS for BiOCuSe at room temperature from (a) backscattering bank (b) 90^{o} bank and (c) low angle bank (average 2θ = 146.7^{o}, 92.6 ^{o} and 52.21^{o} respectively). Key: observed data (red cross); difference curve (blue line); calculated pattern (green line); background (black line) and reflection positions (pink markers).

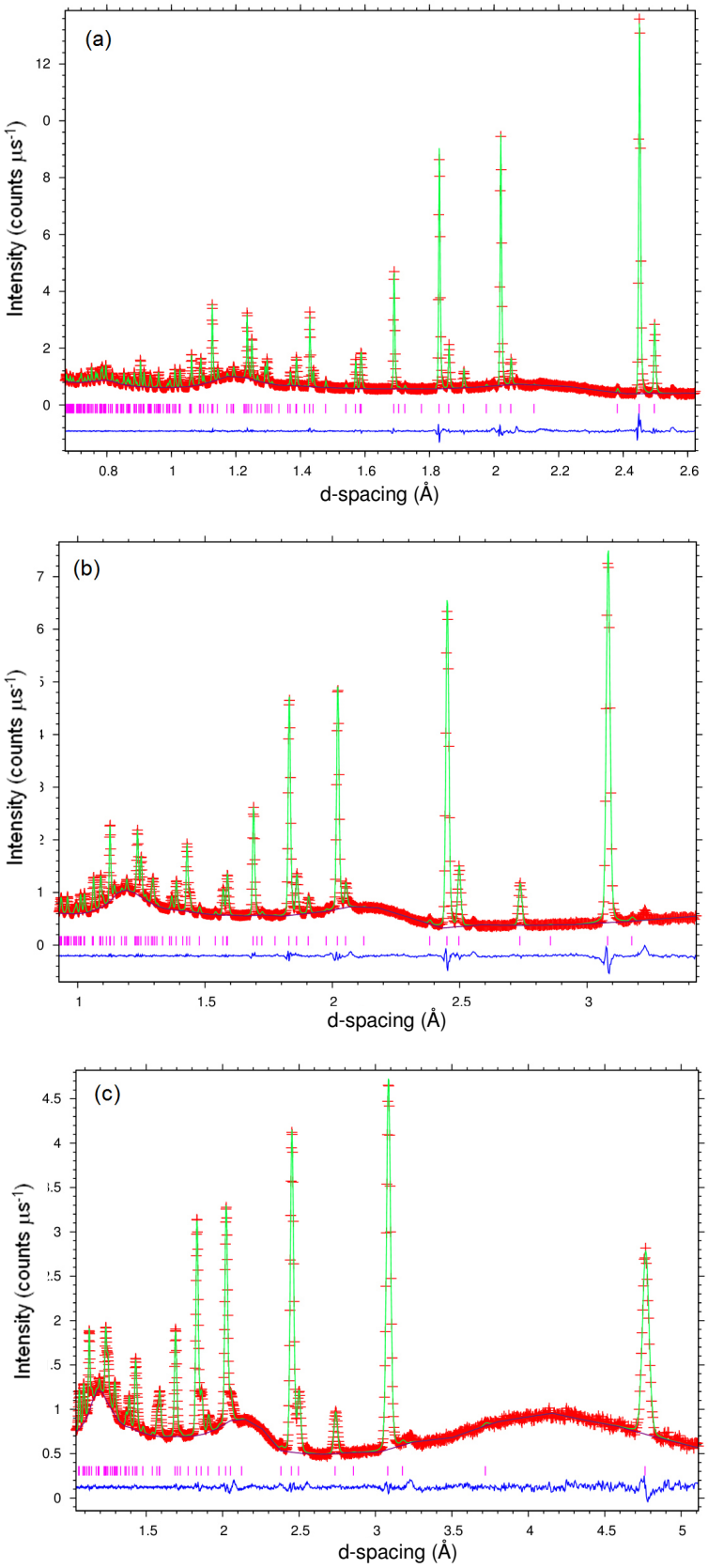

Figure S3. Rietveld refinement using powder neutron diffraction data collected on POLARIS for BiOCuTe at room temperature from (a) backscattering bank (b) 90° bank and (c) low angle bank (average 2θ = 146.7°, 92.6 ° and 52.21° respectively). Key: observed data (red cross); difference curve (blue line); calculated pattern (green line); background (black line) and reflection positions (pink markers).

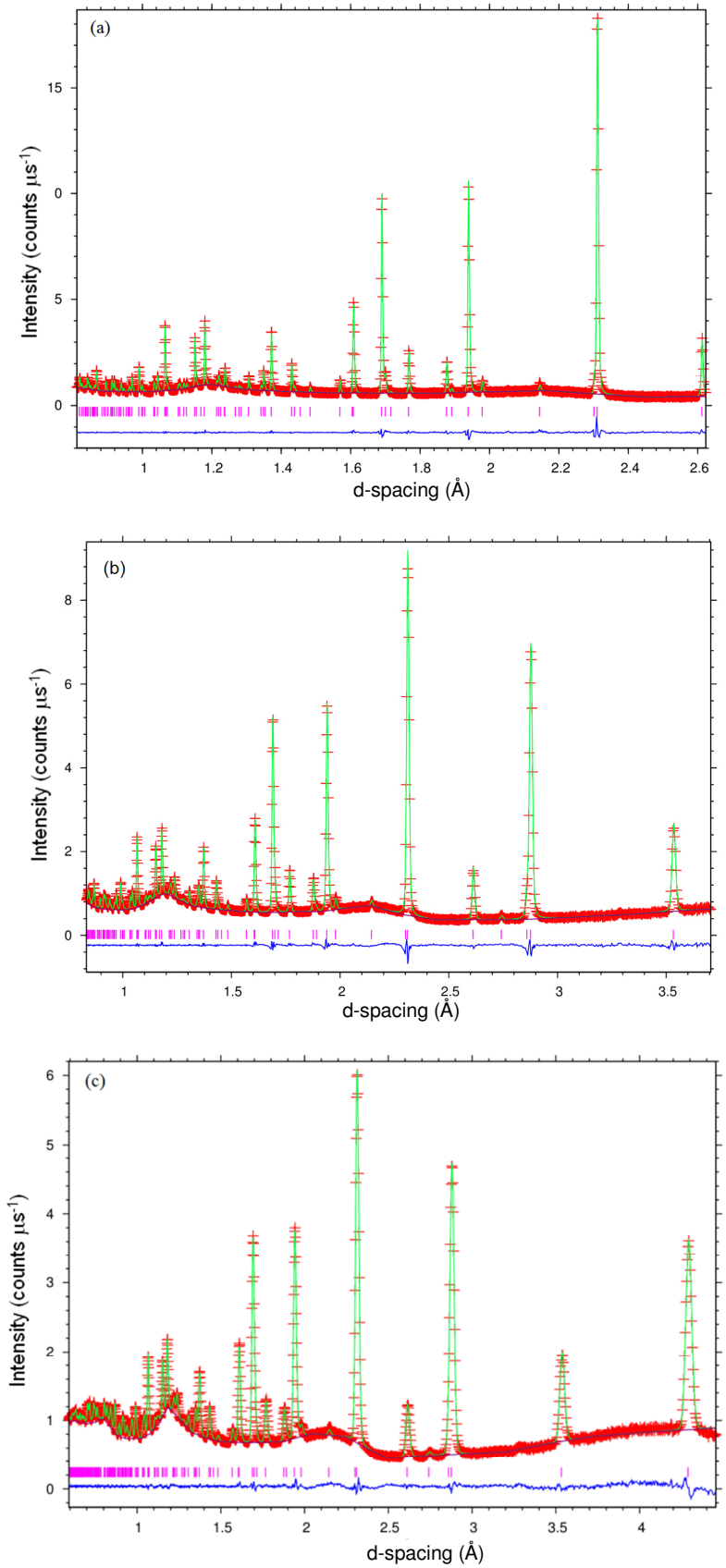

Figure S4. Rietveld refinement using powder neutron diffraction data collected on POLARIS for BiOCuS at 373 K from (a) backscattering bank (b) 90° bank and (c) low angle bank (average 2θ = 146.7°, 92.6 ° and 52.21° respectively). Key: observed data (red cross); difference curve (blue line); calculated pattern (green line); background (black line) and reflection positions (pink markers).

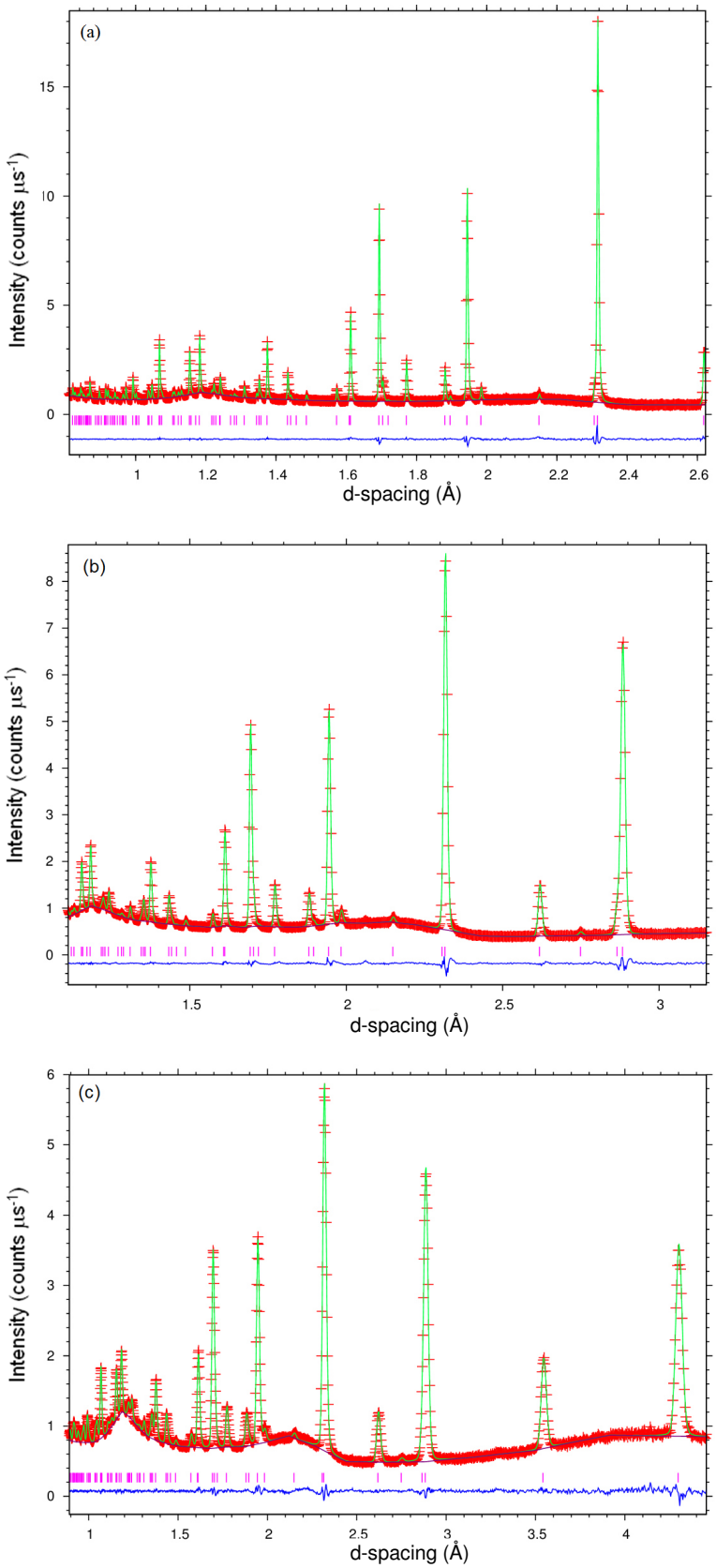

Figure S5. Rietveld refinement using powder neutron diffraction data collected on POLARIS for BiOCuS at 473 K from (a) backscattering bank (b) 90^{o} bank and (c) low angle bank (average 2θ = 146.7^{o}, 92.6 ^{o} and 52.21^{o} respectively). Key: observed data (red cross); difference curve (blue line); calculated pattern (green line); background (black line) and reflection positions (pink markers).

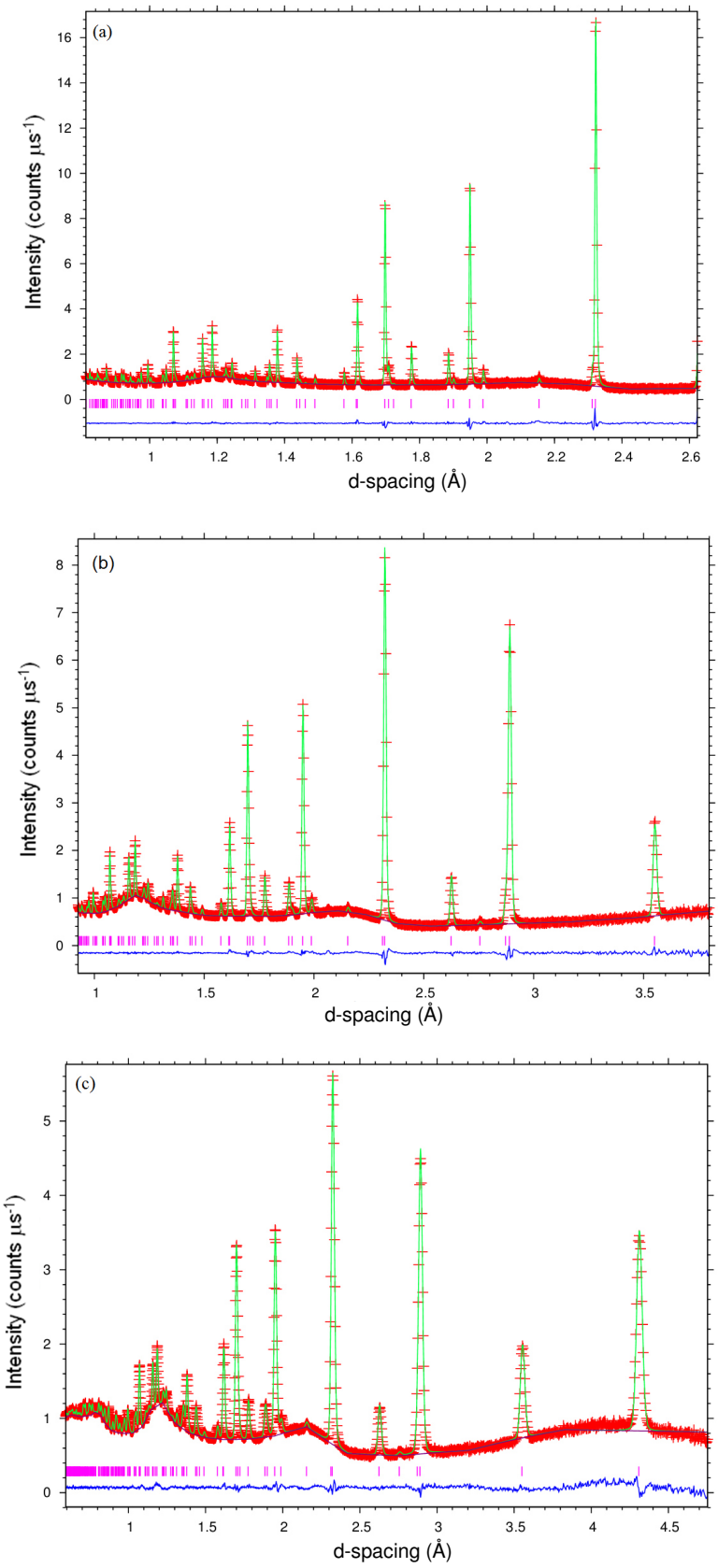

Figure S6. Rietveld refinement using powder neutron diffraction data collected on POLARIS for BiOCuS at 573 K from (a) backscattering bank (b) 90^{o} bank and (c) low angle bank (average 2θ = 146.7^{o}, 92.6 ^{o} and 52.21^{o} respectively). Key: observed data (red cross); difference curve (blue line); calculated pattern (green line); background (black line) and reflection positions (pink markers).

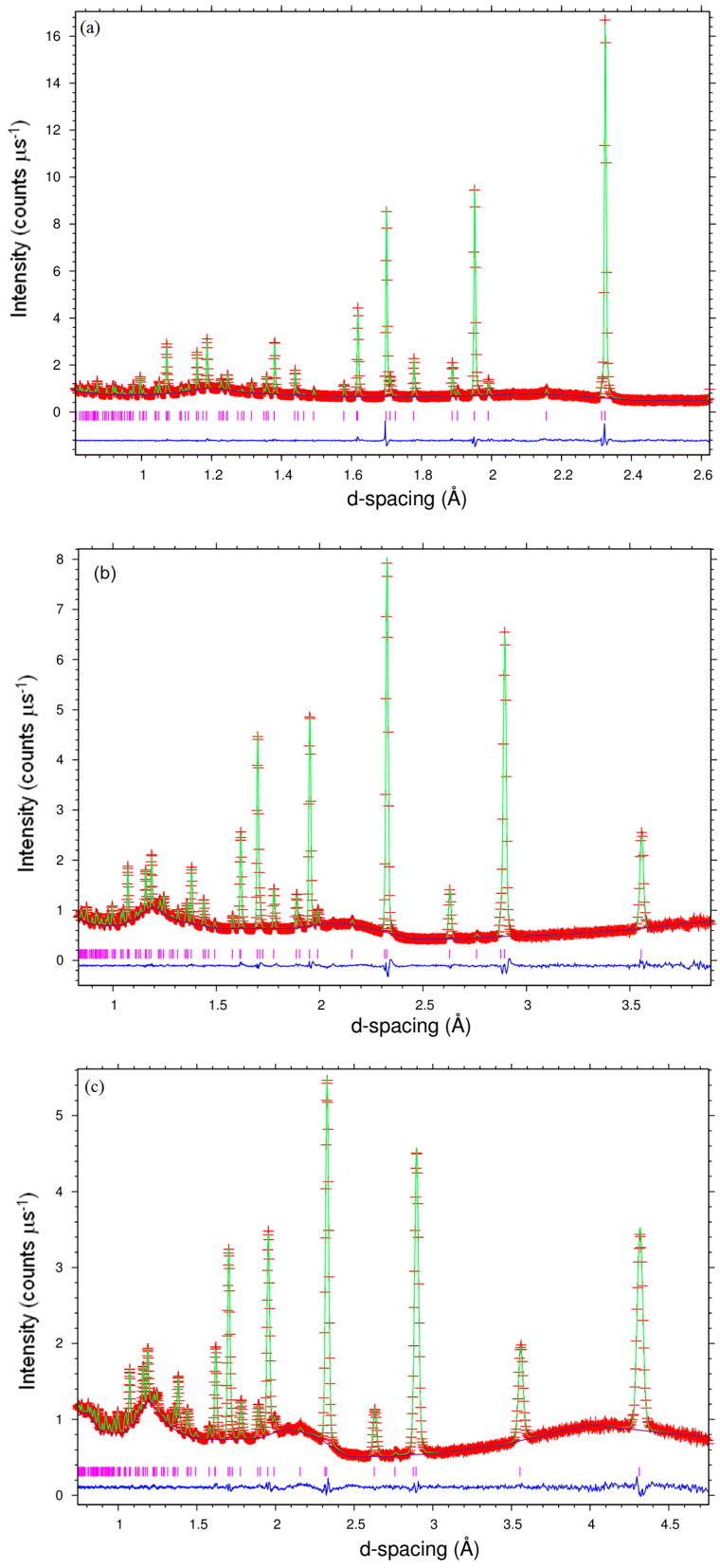

Figure S7. Rietveld refinement using powder neutron diffraction data collected on POLARIS for BiOCuS at 623 K from (a) backscattering bank (b) 90^{o} bank and (c) low angle bank (average 2θ = 146.7^{o}, 92.6 ^{o} and 52.21^{o} respectively). Key: observed data (red cross); difference curve (blue line); calculated pattern (green line); background (black line) and reflection positions (pink markers).

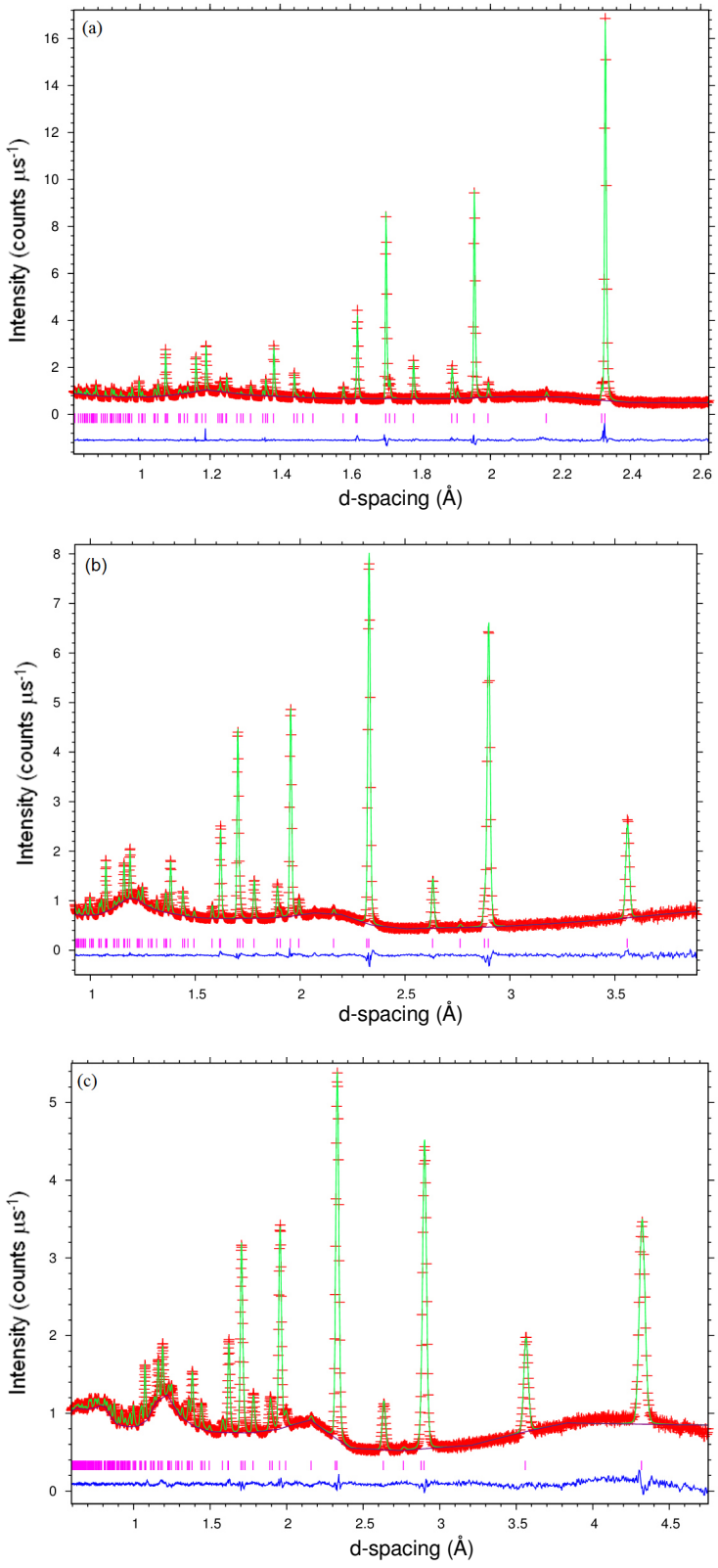

Figure S8. Rietveld refinement using powder neutron diffraction data collected on POLARIS for BiOCuS at 673 K from (a) backscattering bank (b) 90^{o} bank and (c) low angle bank (average 2θ = 146.7^{o}, 92.6 ^{o} and 52.21^{o} respectively). Key: observed data (red cross); difference curve (blue line); calculated pattern (green line); background (black line) and reflection positions (pink markers).

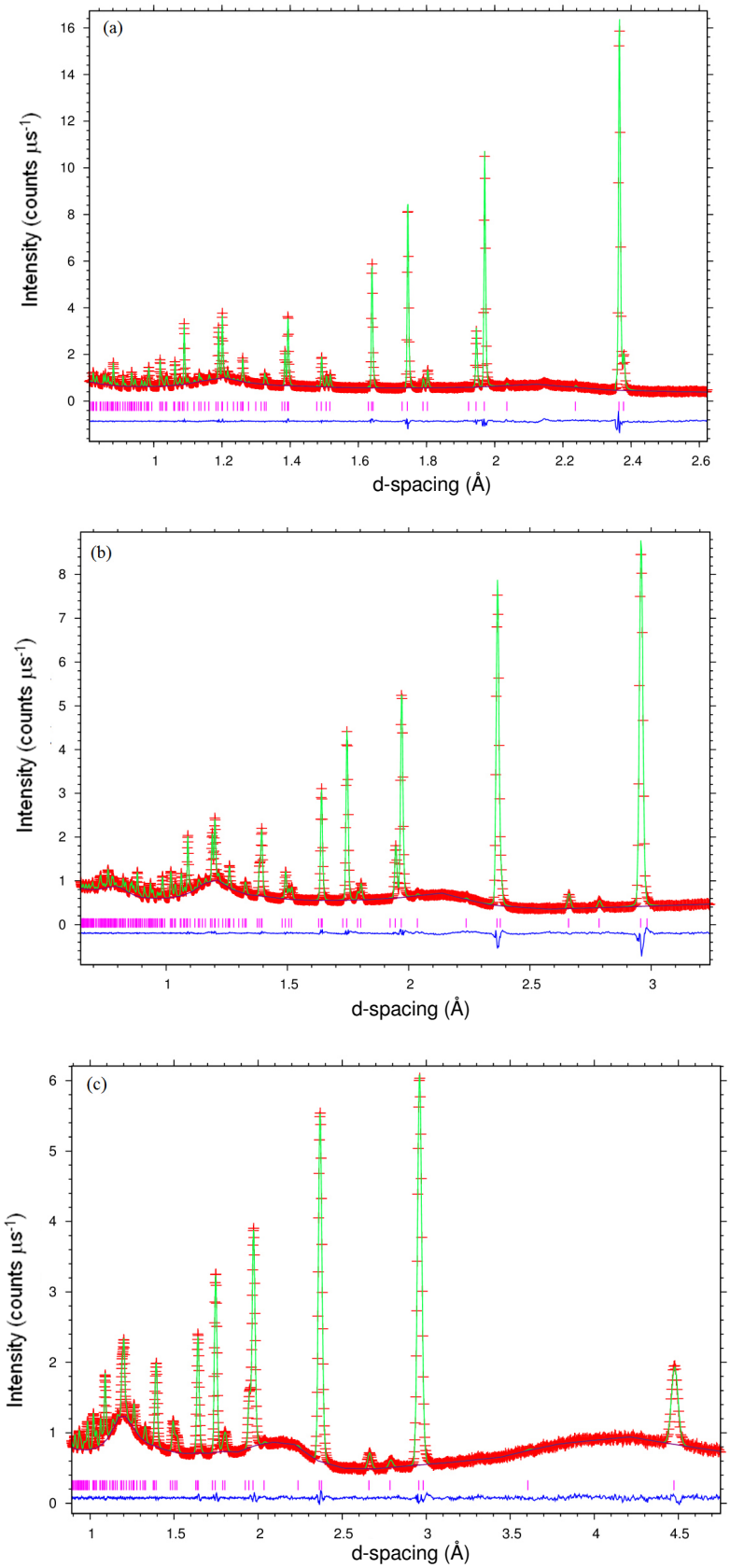

Figure S9. Rietveld refinement using powder neutron diffraction data collected on POLARIS for BiOCuSe at 373 K from (a) backscattering bank (b) 90^{o} bank and (c) low angle bank (average 2θ = 146.7^{o}, 92.6 ^{o} and 52.21^{o} respectively). Key: observed data (red cross); difference curve (blue line); calculated pattern (green line); background (black line) and reflection positions (pink markers).

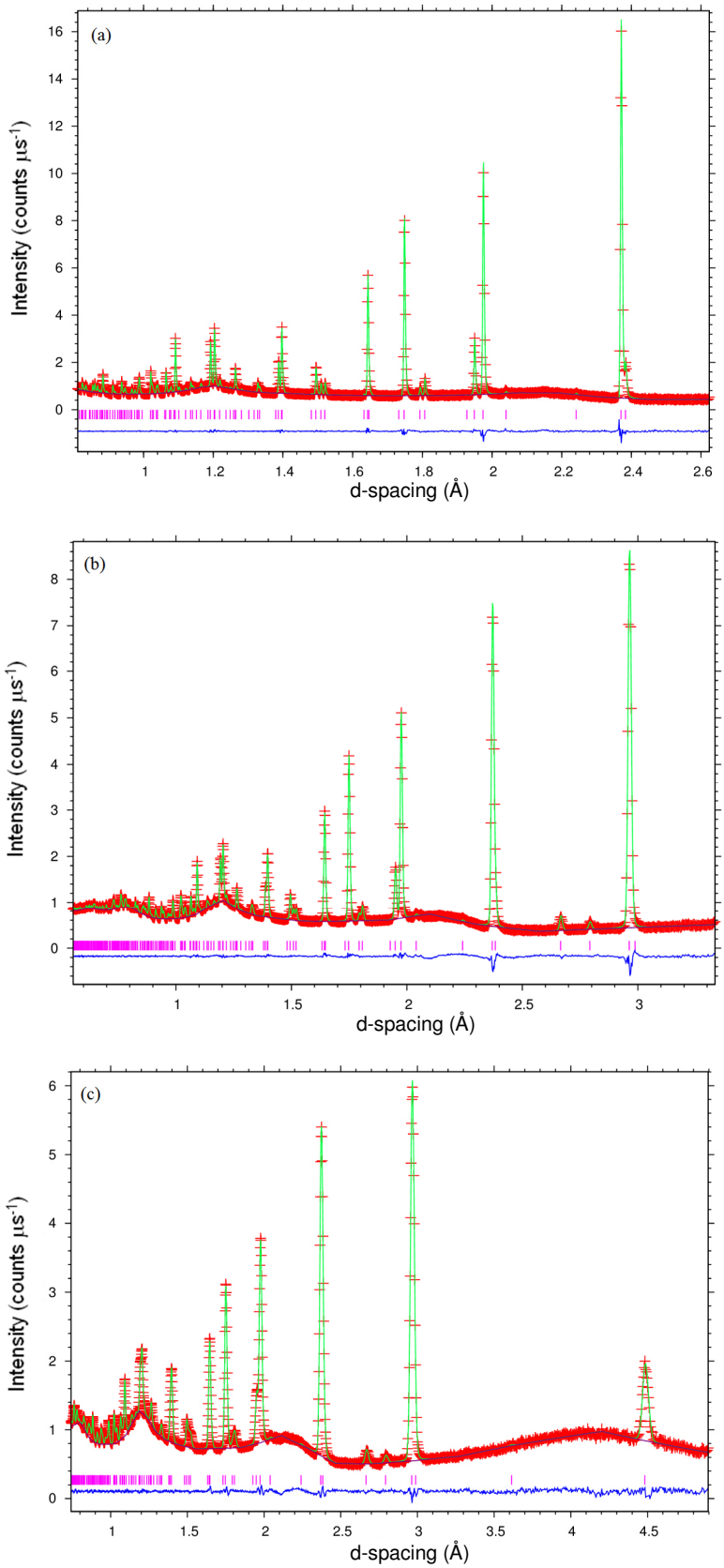

Figure S10. Rietveld refinement using powder neutron diffraction data collected on POLARIS for BiOCuSe at 473 K from (a) backscattering bank (b) 90° bank and (c) low angle bank (average 2θ = 146.7°, 92.6 ° and 52.21° respectively). Key: observed data (red cross); difference curve (blue line); calculated pattern (green line); background (black line) and reflection positions (pink markers).

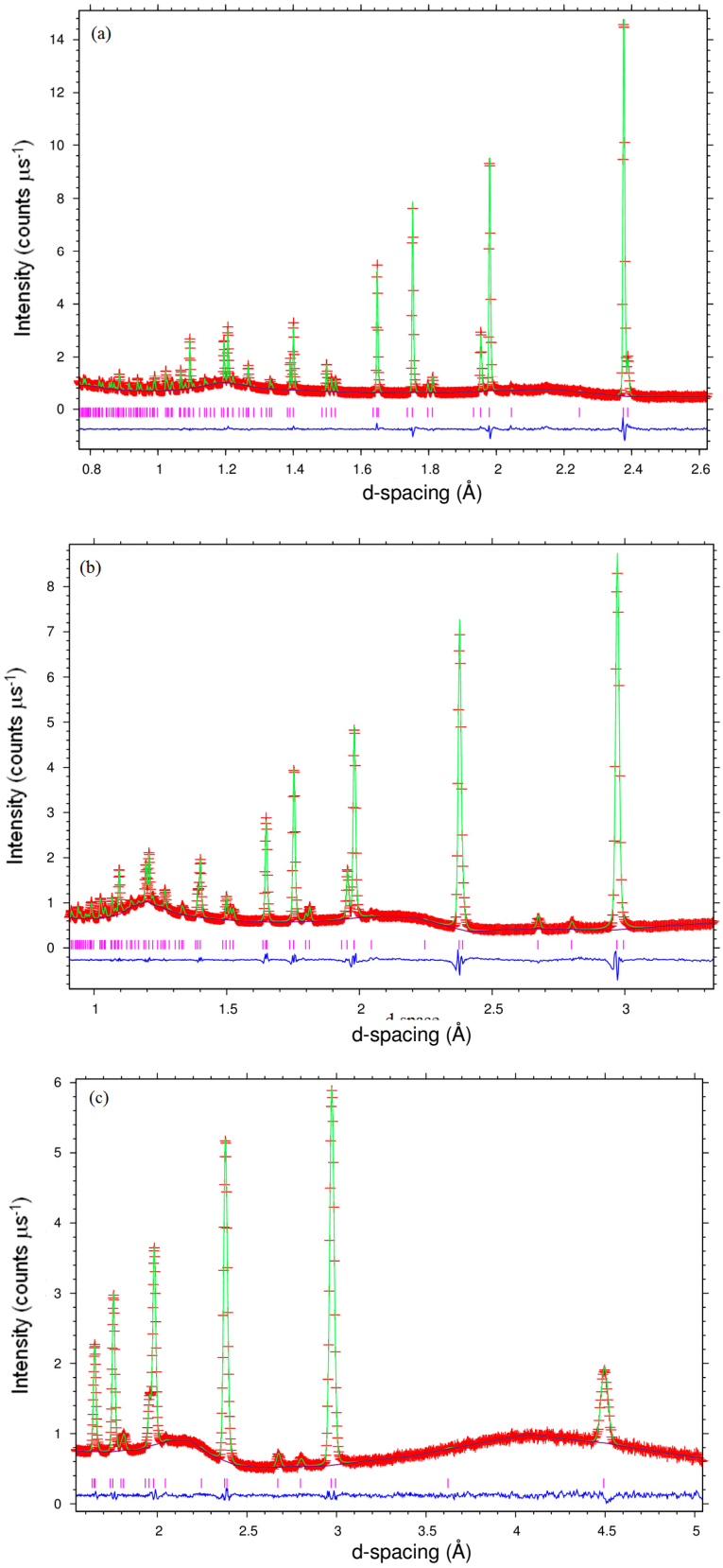

Figure S11. Rietveld refinement using powder neutron diffraction data collected on POLARIS for BiOCuSe at 573 K from (a) backscattering bank (b) 90^{o} bank and (c) low angle bank (average 2θ = 146.7^{o}, 92.6 ^{o} and 52.21^{o} respectively). Key: observed data (red cross); difference curve (blue line); calculated pattern (green line); background (black line) and reflection positions (pink markers).

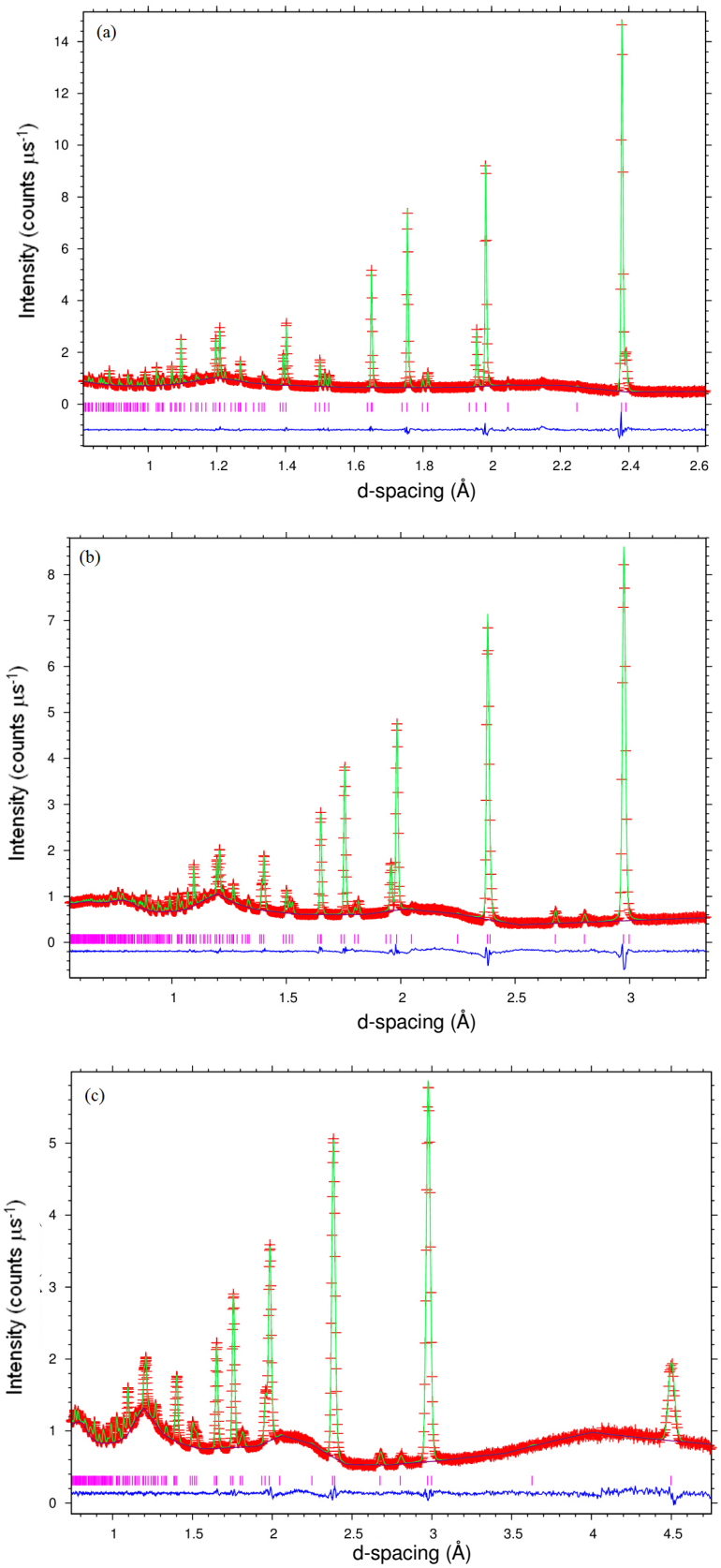

Figure S12. Rietveld refinement using powder neutron diffraction data collected on POLARIS for BiOCuSe at 623 K from (a) backscattering bank (b) 90^{o} bank and (c) low angle bank (average 2θ = 146.7^{o}, 92.6 ^{o} and 52.21^{o} respectively). Key: observed data (red cross); difference curve (blue line); calculated pattern (green line); background (black line) and reflection positions (pink markers).

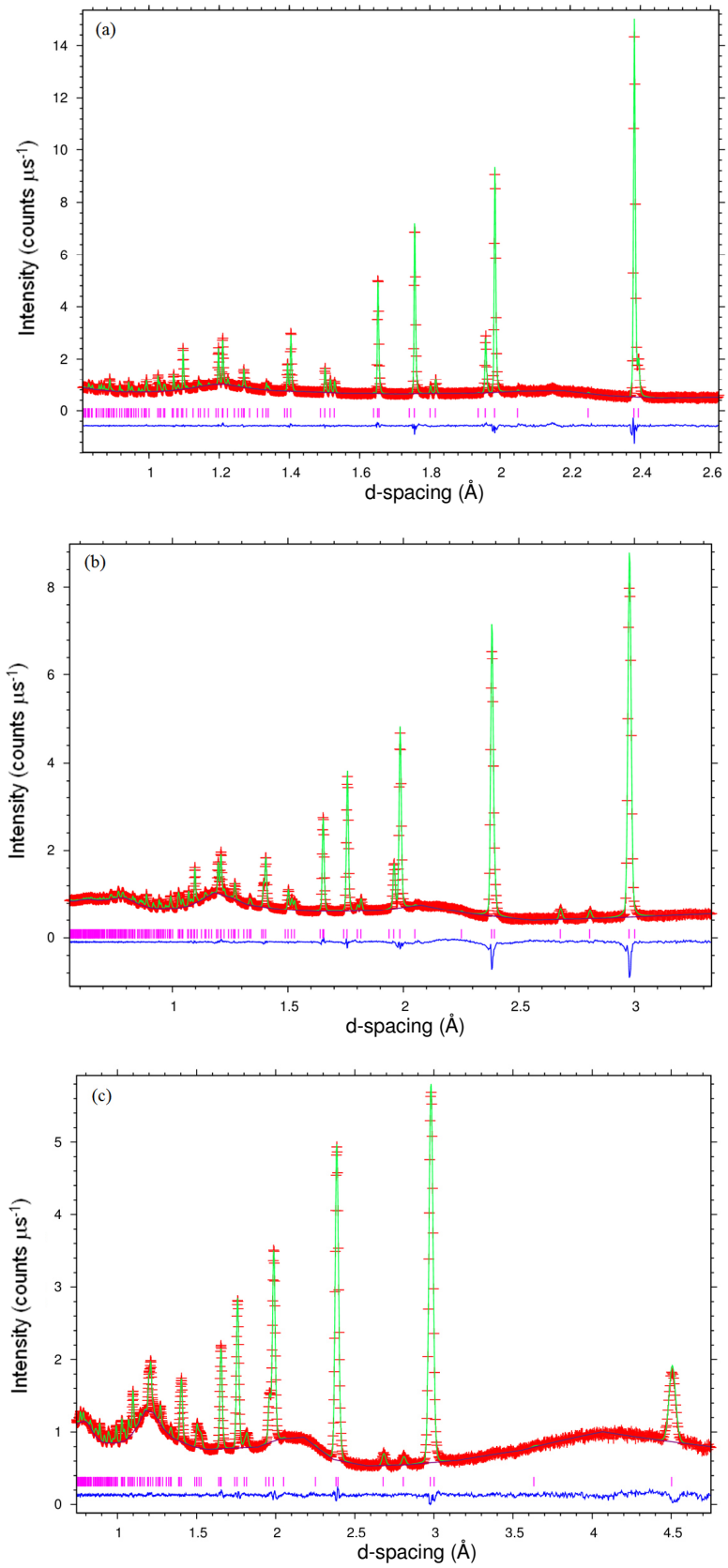

Figure S13. Rietveld refinement using powder neutron diffraction data collected on POLARIS for BiOCuSe at 673 K from (a) backscattering bank (b) 90^{o} bank and (c) low angle bank (average 2θ = 146.7^{o}, 92.6 ^{o} and 52.21^{o} respectively). Key: observed data (red cross); difference curve (blue line); calculated pattern (green line); background (black line) and reflection positions (pink markers).

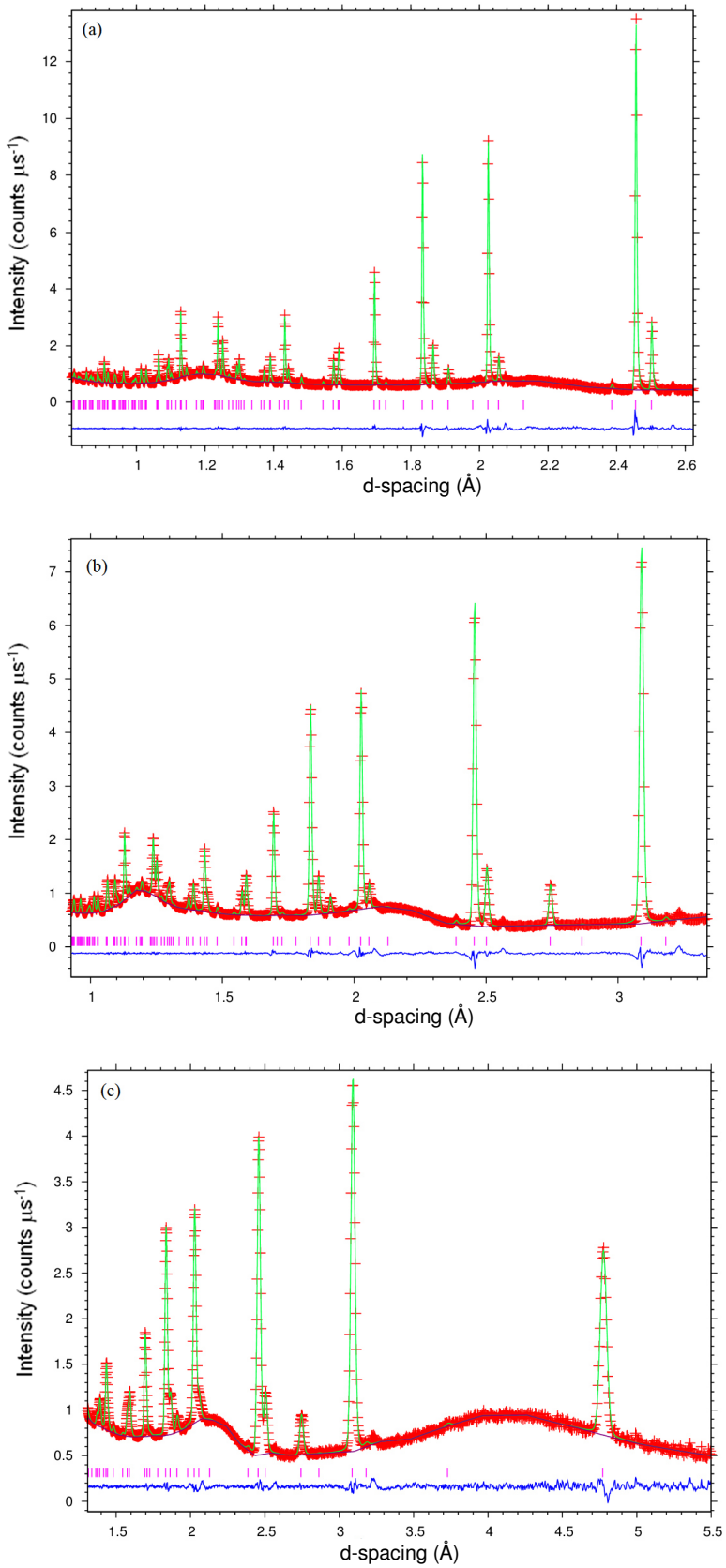

Figure S14. Rietveld refinement using powder neutron diffraction data collected on POLARIS for BiOCuTe at 373 K from (a) backscattering bank (b) 90^{o} bank and (c) low angle bank (average 2θ = 146.7^{o}, 92.6 ^{o} and 52.21^{o} respectively). Key: observed data (red cross); difference curve (blue line); calculated pattern (green line); background (black line) and reflection positions (pink markers).

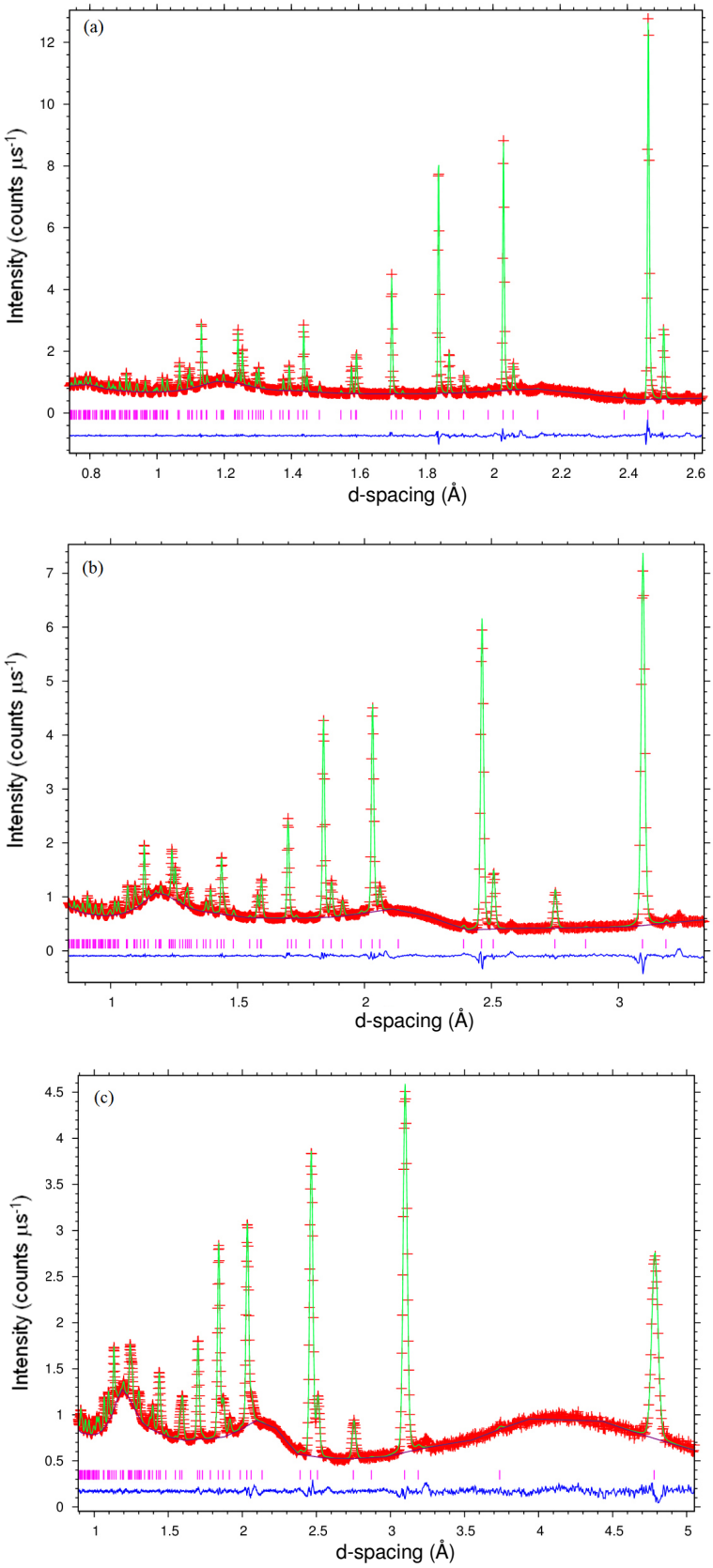

Figure S15. Rietveld refinement using powder neutron diffraction data collected on POLARIS for BiOCuTe at 473 K from (a) backscattering bank (b) 90° bank and (c) low angle bank (average 2θ = 146.7°, 92.6 ° and 52.21° respectively). Key: observed data (red cross); difference curve (blue line); calculated pattern (green line); background (black line) and reflection positions (pink markers).

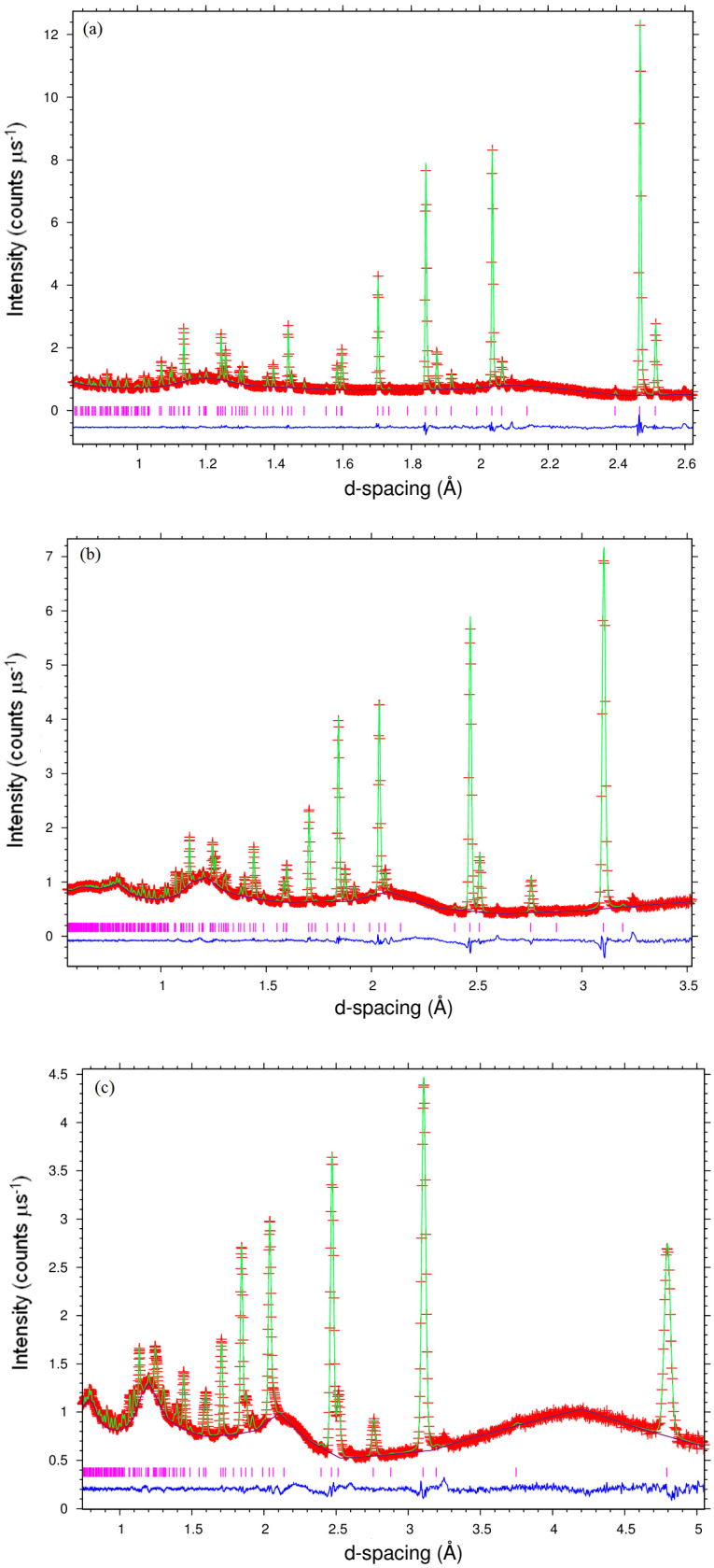

Figure S16. Rietveld refinement using powder neutron diffraction data collected on POLARIS for BiOCuTe at 573 K from (a) backscattering bank (b) 90^{o} bank and (c) low angle bank (average 2θ = 146.7^{o}, 92.6 ^{o} and 52.21^{o} respectively). Key: observed data (red cross); difference curve (blue line); calculated pattern (green line); background (black line) and reflection positions (pink markers).

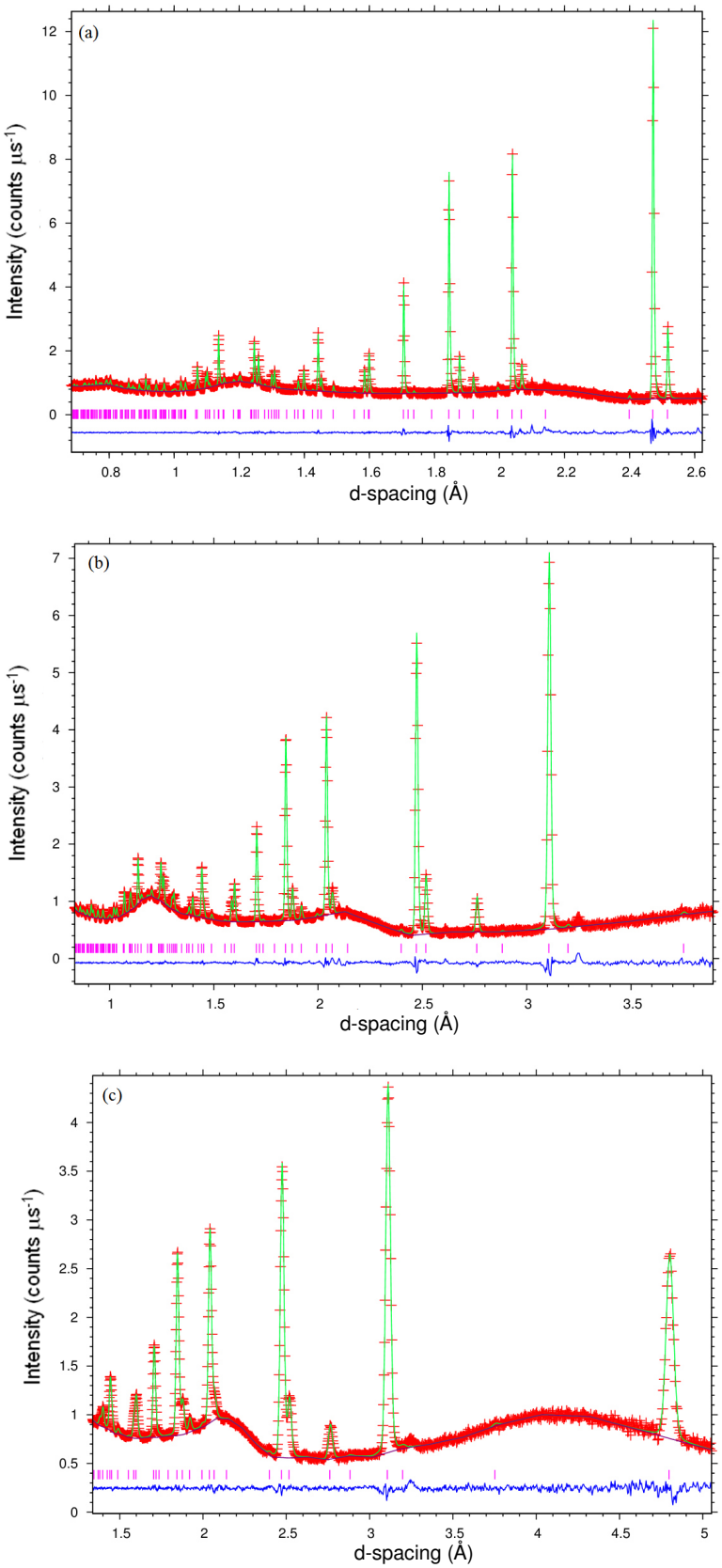

Figure S17. Rietveld refinement using powder neutron diffraction data collected on POLARIS for BiOCuTe at 623 K from (a) backscattering bank (b) 90^{o} bank and (c) low angle bank (average 2θ = 146.7^{o}, 92.6 ^{o} and 52.21^{o} respectively). Key: observed data (red cross); difference curve (blue line); calculated pattern (green line); background (black line) and reflection positions (pink markers).

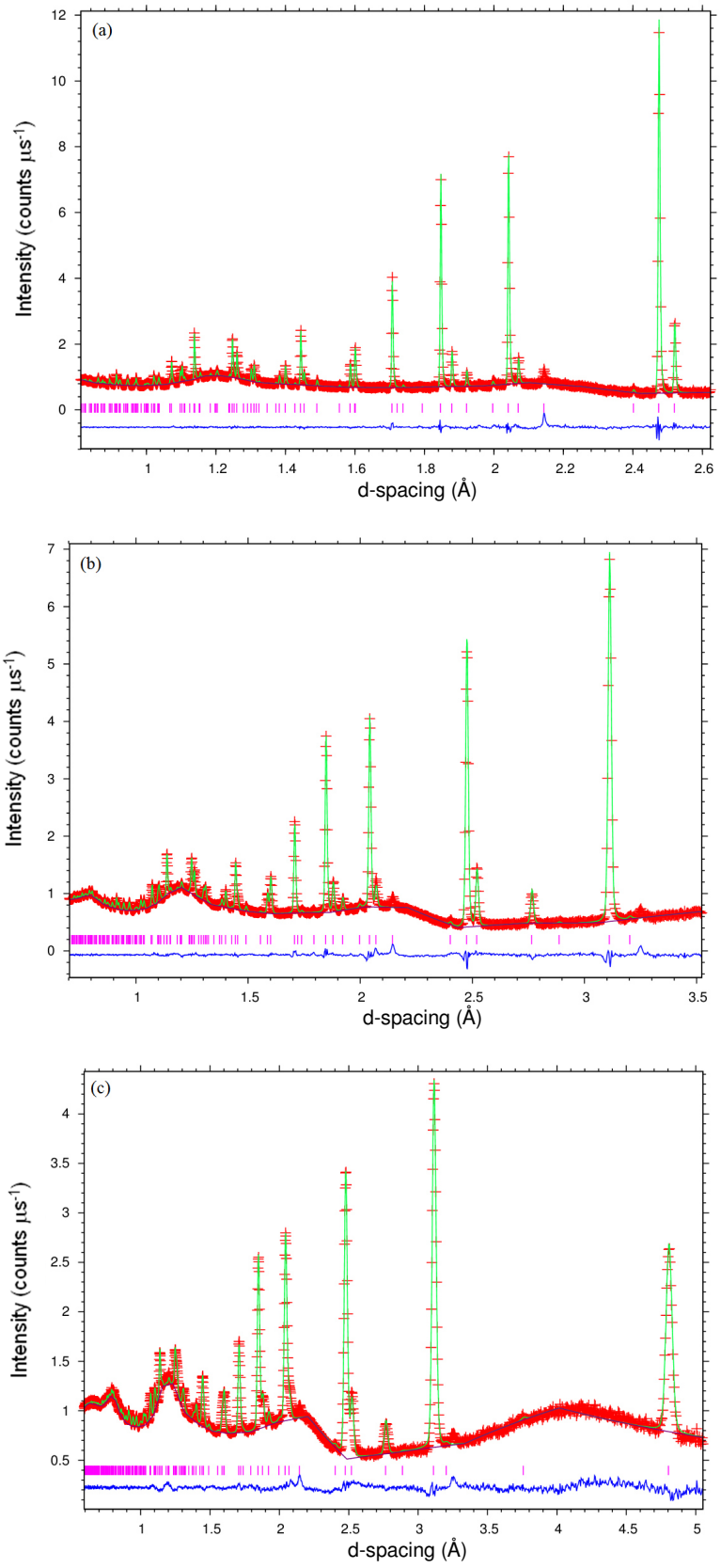

Figure S18. Rietveld refinement using powder neutron diffraction data collected on POLARIS for BiOCuTe at 673 K from (a) backscattering bank (b) 90^{o} bank and (c) low angle bank (average 2θ = 146.7^{o}, 92.6 ^{o} and 52.21^{o} respectively). Key: observed data (red cross); difference curve (blue line); calculated pattern (green line); background (black line) and reflection positions (pink markers).

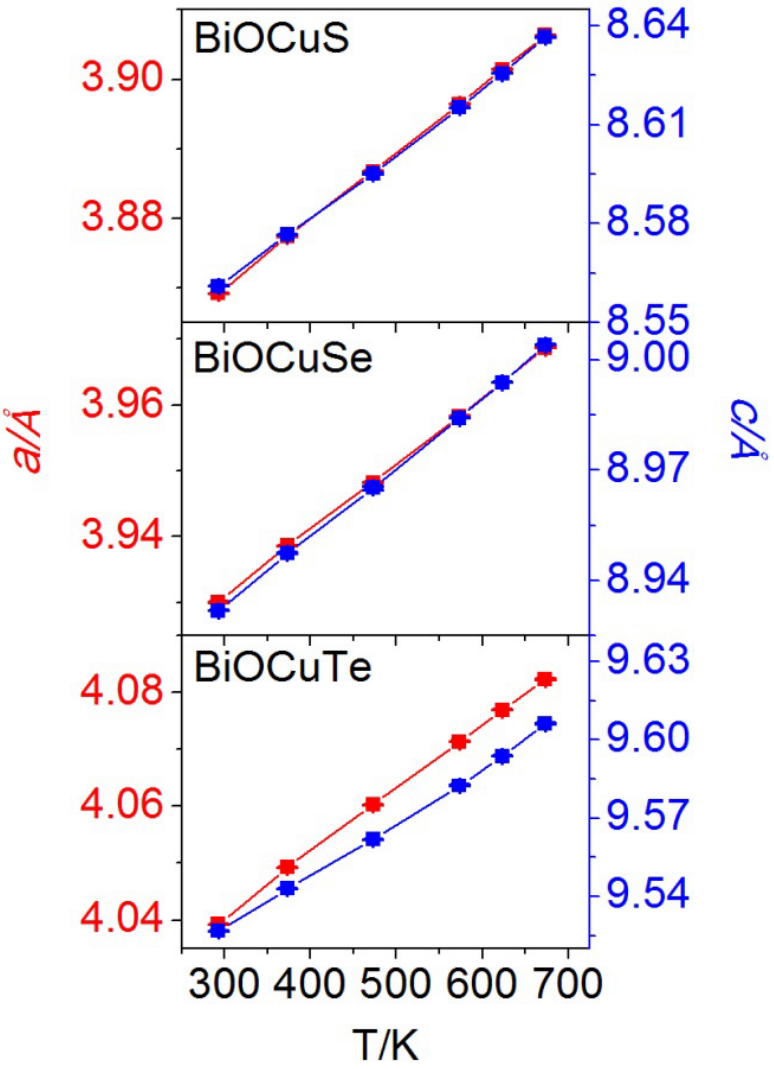

Figure S19. Lattice parameters of BiOCuQ (Q = S, Se, Te) as a function of temperature.

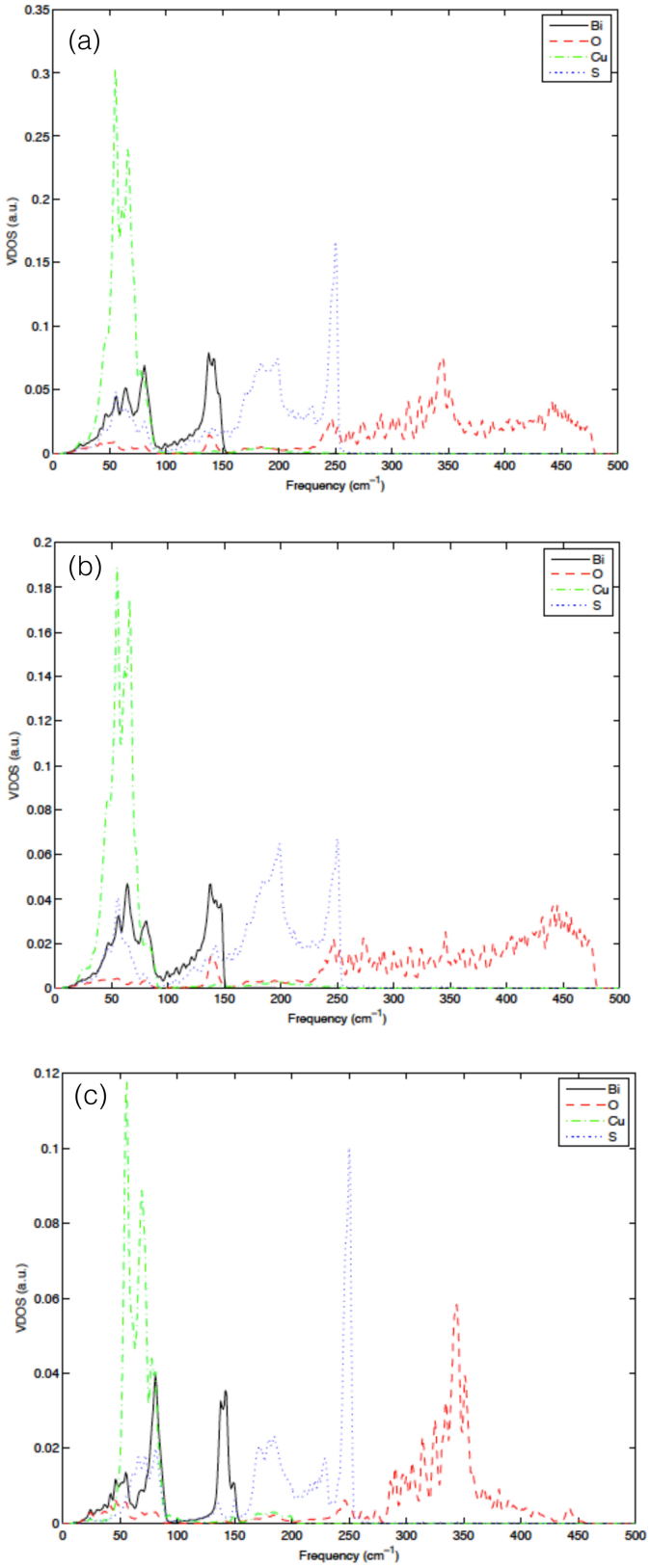

Figure S20. Vibration density of states (VDOS) of BiOCuS. (a) total VDOS projected on each element; (b) in-plane VDOS projected on each element; (c) out-of-plane VDOS projected on each element.

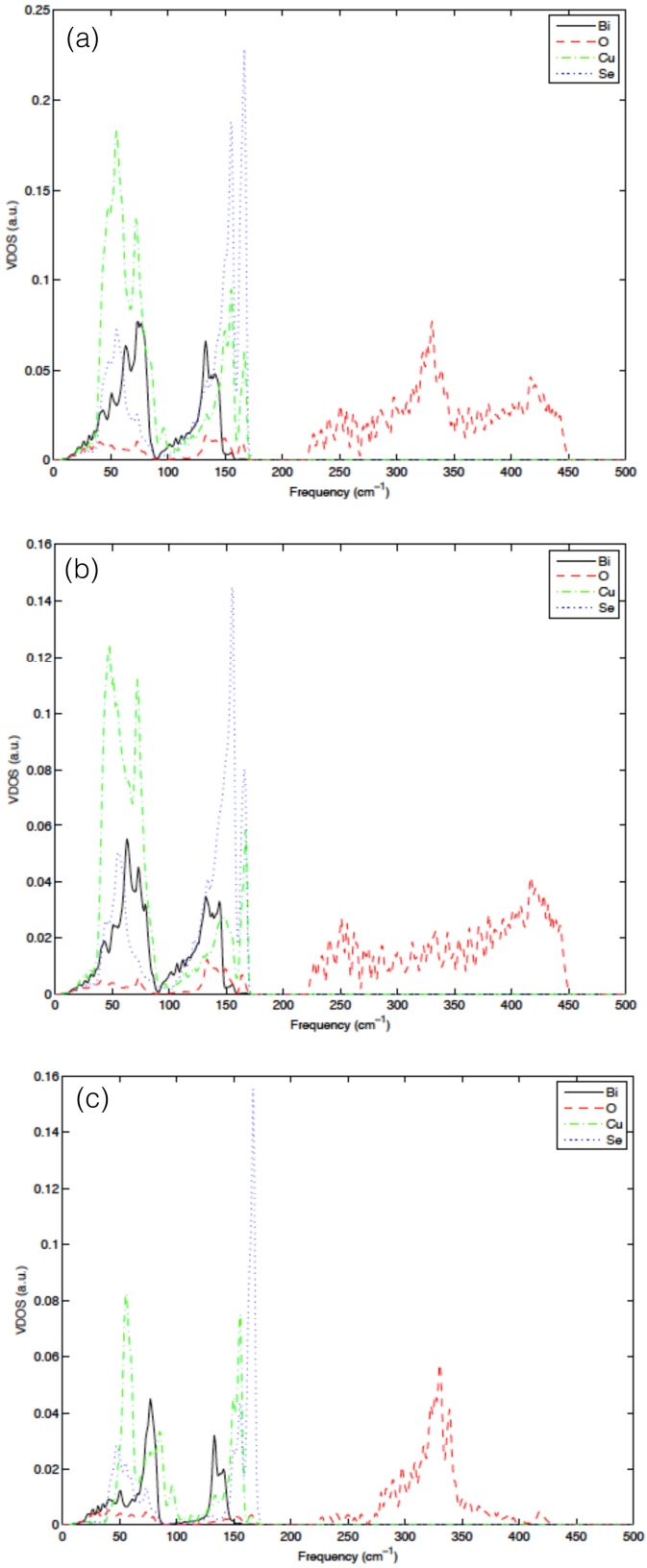

Figure S21. VDOS of BiOCuSe. (a) total projected on each element; (b) in-plane VDOS projected on each element; (c) out-of-plane VDOS projected on each element.

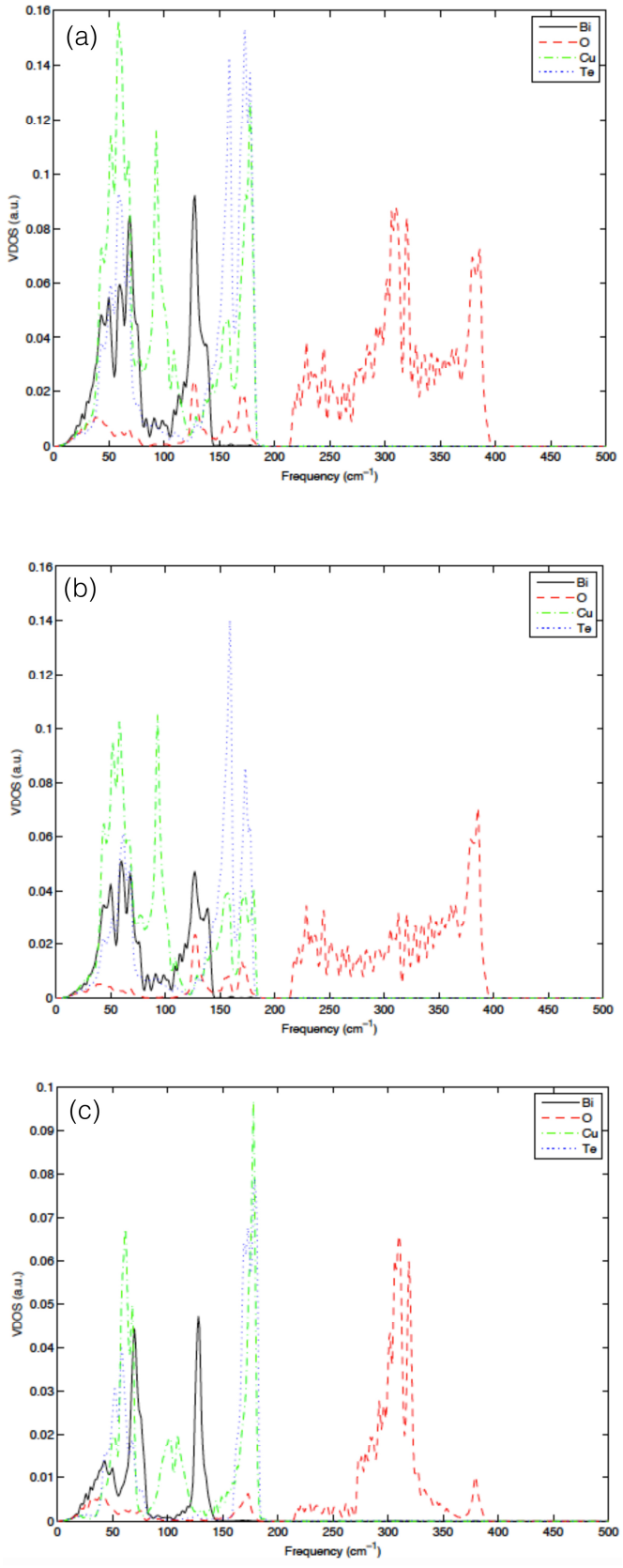

Figure S22. Vibration density of states of BiOCuTe. (a) total projected on each element; (b) in-plane VDOS projected on each element; (c) out-of-plane VDOS projected on each element.

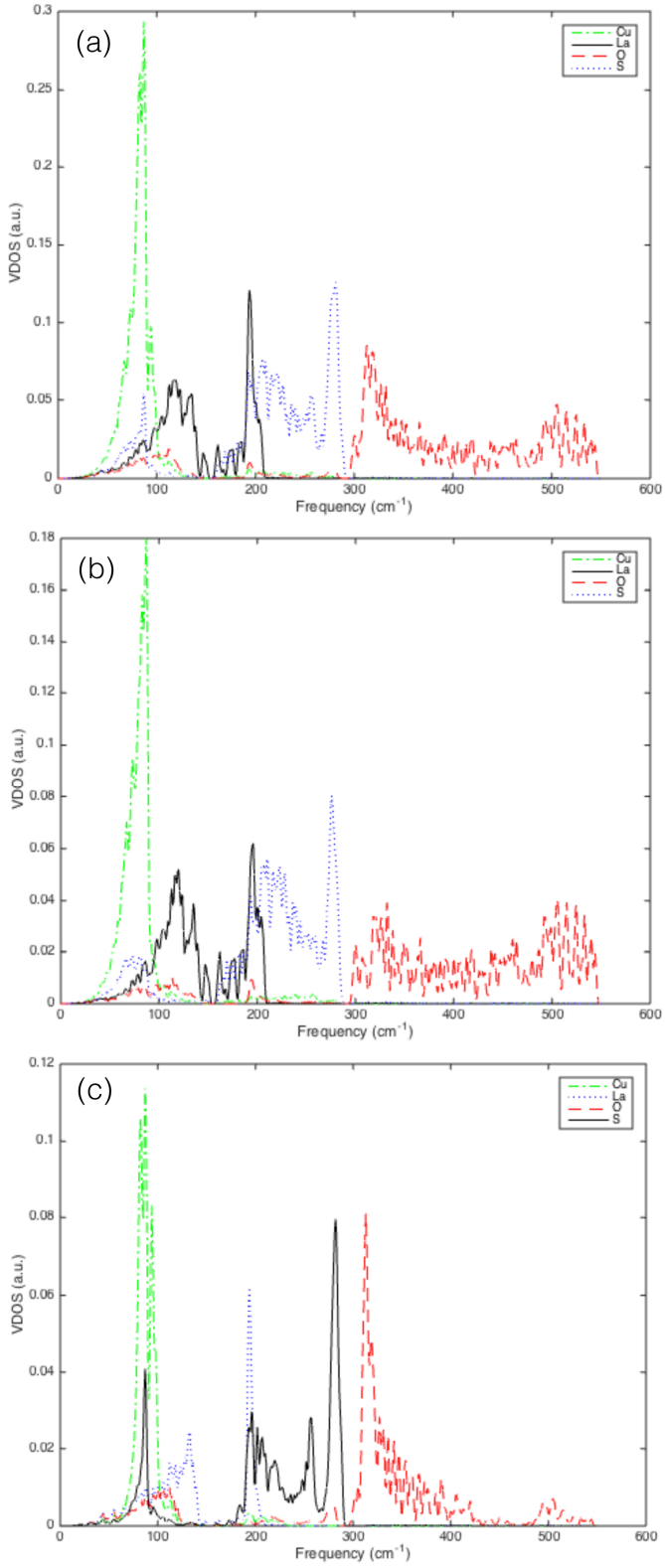

Figure S23. Vibration density of states of LaOCuS. (a) total projected on each element; (b) in-plane VDOS projected on each element; (c) out-of-plane VDOS projected on each element.

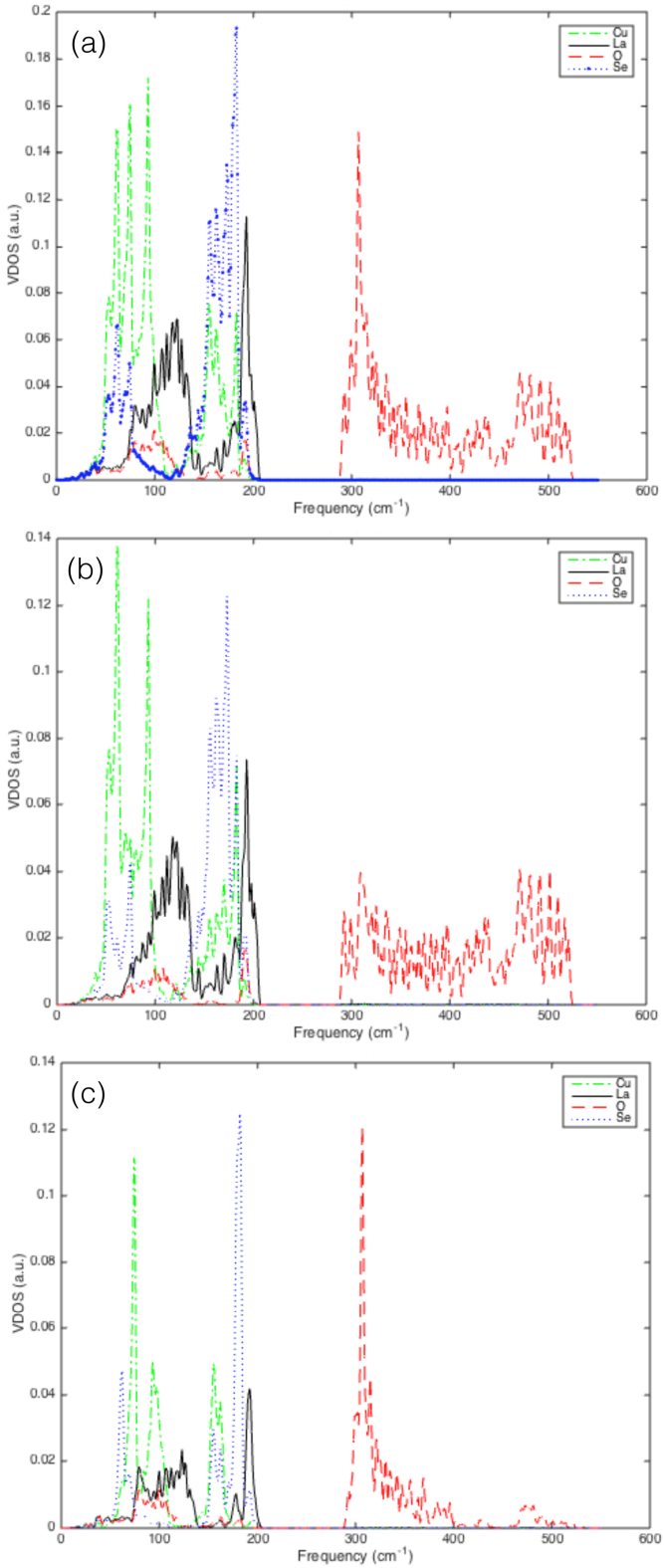

Figure S24. Vibration density of states of LaOCuSe. (a) total projected on each element; (b) in-plane VDOS projected on each element; (c) out-of-plane VDOS projected on each element.

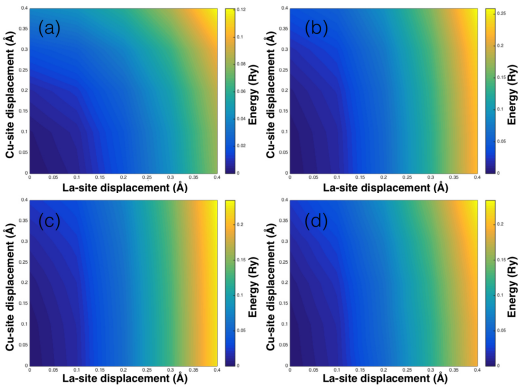

Figure S25 Total energy response to atomic displacements of Bi and Cu in LaCuOS. The displacements were done along inequivalent tetragonal directions: (a) La along x and Cu along x, (b) La along z and Cu along x, (c) La along z and Cu along z, and (d) Bi along +z and Cu along –z.

Table S1. Lattice parameters (*a* & *c*), volume (V), weighted residual error (R_{wp}), Chi-square value (χ^2) for Rietveld refinements of BiOCuS as a function of temperature (Space group: *P*4/*nmm*). Errors are shown as standard deviations.

T (K)	***a* (Å)**	***c* (Å)**	**V(Å^3)**	**R_{wp} (%)**	**χ^2**
293	3.869208(9)	8.561110(38)	128.166(1)	1.46	2.137
373	3.877440(12)	8.576715(47)	128.947(1)	1.59	2.786
473	3.886780(11)	8.595215(45)	129.848(1)	1.48	2.071
573	3.896461(13)	8.615254(50)	130.800(1)	1.50	2.287
623	3.901369(14)	8.625674(56)	131.289(1)	1.53	2.567
673	3.906325(16)	8.636519(63)	131.788(1)	1.71	2.510

Table S2. Lattice parameters (*a* & *c*), volume (V), weighted residual error (R_{wp}), Chi-square value (χ^2) for Rietveld refinements of BiOCuSe as a function of temperature (Space group: *P*4/*nmm*). Errors are shown as standard deviations.

T (K)	***a* (Å)**	***c* (Å)**	**V(Å^3)**	**R_{wp} (%)**	**χ^2**
293	3.930108(11)	8.931876(45)	137.960(1)	1.60	2.917
373	3.938697(11)	8.947477(48)	138.805(1)	1.35	2.786
473	3.948285(13)	8.965107(56)	139.757(1)	1.37	2.545
573	3.958349(16)	8.984095(70)	140.768(1)	1.86	3.394
623	3.963504(16)	8.993851(69)	141.288(1)	1.49	3.046
673	3.968695(17)	9.004077(72)	141.819(1)	1.49	3.057

Table S3. Lattice parameters (*a* & *c*), volume (V), weighted residual error (R_{wp}), Chi-square value (χ^2) for Rietveld refinements of BiOCuTe as a function of temperature (Space group: *P*4/*nmm*). Errors are shown as standard deviations.

T (K)	***a* (Å)**	***c* (Å)**	**V(Å^3)**	**R_{wp} (%)**	**χ^2**
293	4.039197(14)	9.526604(62)	155.428(1)	1.52	2.452
373	4.049215(14)	9.542931(66)	156.467(1)	1.58	2.274
473	4.060234(15)	9.561609(70)	157.628(1)	1.43	2.232
573	4.071338(20)	9.582441(88)	158.837(2)	1.53	3.075
623	4.076905(16)	9.593808(75)	159.460(1)	1.35	1.967
673	4.082304(22)	9.606095(98)	160.088(2)	1.62	3.058

Table S4. Bond lengths and angles for BiOCuS. Errors are shown as standard deviations.

	Bond length			Bond angle			
T (K)	**Bi-O (Å)**	**Bi-S (Å)**	**Cu-S (Å)**	**O-Bi-O (˚)**	**S-Cu-S (˚)**	**S-Cu-S (˚)**	**Cu-S-Cu (˚)**
293	2.31377(27)	3.1517(5)	2.4158(7)	113.467(20)	106.41(4)	111.021(23)	68.979(23)
373	2.31687(31)	3.1557(6)	2.4255(8)	113.604(24)	106.13(5)	111.167(26)	68.833(26)
473	2.32105(33)	3.1664(6)	2.4284(9)	113.710(25)	106.31(5)	111.074(28)	68.926(28)
573	2.32494(34)	3.1742(6)	2.4362(9)	113.853(26)	106.20(6)	111.131(29)	68.869(29)
623	2.3270(4)	3.1784(7)	2.4398(10)	113.917(28)	106.17(6)	111.147(31)	68.853(31)
673	2.3277(4)	3.1820(8)	2.4460(11)	114.089(31)	105.98(7)	111.240(40)	68.760(40)

Table S5. Bond lengths and angles for BiOCuSe. Errors are shown as standard deviations..

	Bond length			Bond angle			
T (K)	**Bi-O (Å)**	**Bi-Se (Å)**	**Cu-Se (Å)**	**O-Bi-O (˚)**	**Se-Cu-Se (˚)**	**Se-Cu-Se (˚)**	**Cu-Se-Cu (˚)**
293	2.32834(23)	3.23122(33)	2.51425(31)	115.124(18)	102.808(17)	112.902(9)	67.098(9)
373	2.33234(23)	3.23851(34)	2.51951(31)	115.208(18)	102.822(17)	112.895(9)	67.105(9)
473	2.33626(27)	3.2479(4)	2.5245(4)	115.344(21)	102.886(20)	112.861(11)	67.139(11)
573	2.3389(4)	3.2593(5)	2.5298(5)	115.600(28)	102.951(28)	112.826(15)	67.174(15)
623	2.34141(33)	3.2643(5)	2.5322(4)	115.643(26)	103.001(25)	112.800(13)	67.200(13)
673	2.3442(4)	3.2689(5)	2.5350(5)	115.668(28)	103.030(27)	112.785(14)	67.215(14))

Table S6. Bond lengths and angles for BiOCuTe. Errors are shown as standard deviations.

	Bond length			Bond angle			
T (K)	**Bi-O (Å)**	**Bi-Te (Å)**	**Cu-Te (Å)**	**O-Bi-O (˚)**	**Te-Cu-Te (˚)**	**Te-Cu-Te (˚)**	**Cu-Te-Cu (˚)**
293	2.35532(28)	3.3953(5)	2.6498(5)	118.066(22)	99.310(25)	114.779(14)	65.221(14)
373	2.35988(33)	3.4052(6)	2.6539(6)	118.169(27)	99.440(29)	114.708(15)	65.292(15)
473	2.36495(34)	3.4150(6)	2.6598(6)	118.279(28)	99.507(29)	114.672(16)	65.328(16)
573	2.3677(4)	3.4302(8)	2.6631(7)	118.579(35)	99.71(4)	114.564(20)	65.436(20)
623	2.3723(4)	3.4327(7)	2.6670(7)	118.471(33)	99.692(34)	114.571(18)	65.429(18)
673	2.3756(5)	3.4353(9)	2.6725(8)	118.46(4)	99.59(4)	114.624(22)	65.376(22)

Table S7. Site occupancy factors (SOF), coordinates, and atomic displacement parameters (U_{iso}) for BiOCuS as a function of temperature (Space group: *P*4/*nmm*). Errors are shown as standard deviations.

T (K)	**Atom**	**SOF**	***x***	***y***	***z***	**U_{iso}(Å^2)**
293	Bi	1.0	1/4	1/4	0.148250(57)	0.00655(9)
	O	1.0	3/4	1/4	0	0.00579(14)
	Cu	1.0	3/4	1/4	½	0.01599(14)
	S	1.0	1/4	1/4		0.00737(30)
373	Bi	1.0	1/4	1/4	0.147908 (66)	0.00931(10)
	O	1.0	3/4	1/4	0	0.00764(16)
	Cu	1.0	3/4	1/4	½	0.0223(17)
	S	1.0	1/4	1/4	0.669771(159)	0.01085(35)
473	Bi	1.0	1/4	1/4	0.147646(70)	0.01292(12)
	O	1.0	3/4	1/4	0	0.01014(18)
	Cu	1.0	3/4	1/4	½	0.03126(20)
	S	1.0	1/4	1/4	0.669420(168)	0.01494(39)
573	Bi	1.0	1/4	1/4	0.147269(72)	0.01670(13)
	O	1.0	3/4	1/4	0	0.01235(18)
	Cu	1.0	3/4	1/4	½	0.04012(23)
	S	1.0	1/4	1/4	0.669785(173)	0.01664(40)
623	Bi	1.0	1/4	1/4	0.147097(77)	0.01803(14)
	O	1.0	3/4	1/4	0	0.01442(20)
	Cu	1.0	3/4	1/4	½	0.04513(27)
	S	1.0	1/4	1/4	0.669894(188)	0.01942(43)
673	Bi	1.0	1/4	1/4	0.146614(86)	0.02035(16)
	O	1.0	3/4	1/4	0	0.01506(22)
	Cu	1.0	3/4	1/4	½	0.04983(31)
	S	1.0	1/4	1/4	0.670482(211)	0.02049(49)

Table S8. Site occupancy factors (SOF), coordinates, and atomic displacement parameters (U_{iso}) for BiOCuSe as a function of temperature (Space group: *P*4/*nmm*). Errors are shown as standard deviations.

T (K)	**Atom**	**SOF**	***x***	***y***	***z***	**U_{iso}(Å^2)**
293	Bi	1.0	1/4	1/4	0.139824(47)	0.00712(14)
	O	1.0	3/4	1/4	0	0.00648(18)
	Cu	1.0	3/4	1/4	1/2	0.01474(17)
	Se	1.0	1/4	1/4	0.675421(58)	0.00688(15)
373	Bi	1.0	1/4	1/4	0.139658(48)	0.01013(13)
	O	1.0	3/4	1/4	0	0.00856(17)
	Cu	1.0	3/4	1/4	1/2	0.02091(17)
	Se	1.0	1/4	1/4	0.675636(55)	0.00965(14)
473	Bi	1.0	1/4	1/4	0.139357 (55)	0.01384(16)
	O	1.0	3/4	1/4	0	0.01151(20)
	Cu	1.0	3/4	1/4	1/2	0.02881(22)
	Se	1.0	1/4	1/4	0.675516(63)	0.01293(17)
573	Bi	1.0	1/4	1/4	0.138728 (75)	0.01662(27)
	O	1.0	3/4	1/4	0	0.01318(30)
	Cu	1.0	3/4	1/4	1/2	0.03632(34)
	Se	1.0	1/4	1/4	0.675179(145)	0.01484(26)
623	Bi	1.0	1/4	1/4	0.138643(69)	0.01918(22)
	O	1.0	3/4	1/4	0	0.01583(26)
	Cu	1.0	3/4	1/4	1/2	0.04252(32)
	Se	1.0	1/4	1/4	0.675268(80)	0.01791(23)
673	Bi	1.0	1/4	1/4	0.138600(76)	0.02394(24)
	O	1.0	3/4	1/4	0	0.01707(28)
	Cu	1.0	3/4	1/4	1/2	0.04982(33)
	Se	1.0	1/4	1/4	0.675206(85)	0.02060(24)

Table S9. Site occupancy factors (SOF), coordinates, and atomic displacement parameters (U_{iso}) for BiOCuTe as a function of temperature (Space group: *P*4/*nmm*). Errors are shown as standard deviations.

T (K)	**Atom**	**SOF**	***x***	***y***	***z***	**U_{iso}(Å^2)**
293	Bi	1.0	1/4	1/4	0.127214(56)	0.01056(13)
	O	1.0	3/4	1/4	0	0.00761(16)
	Cu	1.0	3/4	1/4	1/2	0.01567(15)
	Te	1.0	1/4	1/4	0.680072(81)	0.00908(17)
373	Bi	1.0	1/4	1/4	0.127051(68)	0.01472(18)
	O	1.0	3/4	1/4	0	0.01027(20)
	Cu	1.0	3/4	1/4	1/2	0.02227(21)
	Te	1.0	1/4	1/4	0.679797(91)	0.01221(22)
473	Bi	1.0	1/4	1/4	0.126873(69)	0.01928(18)
	O	1.0	3/4	1/4	0	0.01423(21)
	Cu	1.0	3/4	1/4	1/2	0.03128(24)
	Te	1.0	1/4	1/4	0.679721(92)	0.01643(22)
573	Bi	1.0	1/4	1/4	0.126188(88)	0.02523(23)
	O	1.0	3/4	1/4	0	0.01813(27)
	Cu	1.0	3/4	1/4	1/2	0.04196(32)
	Te	1.0	1/4	1/4	0.679188(117)	0.01972(27)
623	Bi	1.0	1/4	1/4	0.126482(82)	0.02747(22)
	O	1.0	3/4	1/4	0	0.01988(25)
	Cu	1.0	3/4	1/4	1/2	0.04719(34)
	Te	1.0	1/4	1/4	0.679263(108)	0.02267(27)
673	Bi	1.0	1/4	1/4	0.126528(100)	0.02973(27)
	O	1.0	3/4	1/4	0	0.02245(32)
	Cu	1.0	3/4	1/4	1/2	0.05344(39)
	Te	1.0	1/4	1/4	0.679583(131)	0.02453(34)

Table S10**.** Born effective charges computed with density functional perturbation theory for MOCuS (M = Bi, La). In plane (xx) and out of plane (zz) components are given as xx/zz.

Material	M	O	Cu	S
BiOCuS	5.97/5.70	-3.82/-4.02	1.17/0.65	-3.29/-2.40
LaOCuS	4.60/4.75	-3.09/-4.45	0.95/0.23	-2.44/-1.62